Learning Where to Learn in Cross-View Self-Supervised Learning

Lang Huang[1], Shan You[2]*, Mingkai Zheng[3], Fei Wang[2], Chen Qian[2], Toshihiko Yamasaki[1]

[1]The University of Tokyo; [2]SenseTime Research; [3]The University of Sydney

{langhuang,yamasaki}@cvm.t.u-tokyo.ac.jp

{youshan,wangfei,qianchen}@sensetime.com, mzhe4001@uni.sydney.edu.au

Abstract

*Self-supervised learning (SSL) has made enormous progress and largely narrowed the gap with the supervised ones, where the representation learning is mainly guided by a projection into an embedding space. During the projection, current methods simply adopt uniform aggregation of pixels for embedding; however, this risks involving object-irrelevant nuisances and spatial misalignment for different augmentations. In this paper, we present a new approach, **Le**arning **Whe**re to **L**earn (LEWEL), to adaptively aggregate spatial information of features, so that the projected embeddings could be exactly aligned and thus guide the feature learning better. Concretely, we reinterpret the projection head in SSL as a per-pixel projection and predict a set of spatial alignment maps from the original features by this weight-sharing projection head. A spectrum of aligned embeddings is thus obtained by aggregating the features with spatial weighting according to these alignment maps. As a result of this adaptive alignment, we observe substantial improvements on both image-level prediction and dense prediction at the same time: LEWEL improves MoCov2 [15] by 1.6%/1.3%/0.5%/0.4% points, improves BYOL [14] by 1.3%/1.3%/0.7%/0.6% points, on ImageNet linear/semi-supervised classification, Pascal VOC semantic segmentation, and object detection, respectively.[†]*

1. Introduction

In recent years, self-supervised learning (SSL) [7, 12, 14, 15, 29, 30, 42] has attained tremendous attention due to its impressive ability to learn good representations from large volume of unlabeled data. Among them, the state-of-the-art instance discrimination approaches [7, 14, 15, 30, 42] encourage the representation learning with image-level invariance to a set of random data transformations, *e.g.*, random cropping and color distortions. These methods even exhibit superior performance over their supervised counter-

parts for various downstream tasks, such as object detection [11, 25] and semantic segmentation [11]. There remain, however, several important issues unresolved. Two of them are mainly attributed to the rigorous invariance to random cropping because it would risk introducing more irrelevant nuisance (*e.g.*, background information) and spatial misalignment of objects for augmentations. Though, for SSL, random cropping might be the most effective data augmentation option [7] and a good degree of spatial misalignment is beneficial [38], it remains unclear how to choose the optimal degree of misalignment. Furthermore, the involved nuisance will hinder the discrimination ability of image-level representations while the misalignment discards some important spatial information of objects.

Several recent literatures have dedicated to alleviating these issues by involving some localization priors of downstream tasks in advance. For example, the works of [40, 44] explored pixel-level consistency between two augmented views, while some other works proposed to match the representation of a set of pre-defined bounding-boxes [35, 43] or pre-computed masks [19] between the two views. Despite the improved performance on dense prediction tasks, these methods still suffer from several drawbacks, *e.g.*, they rely on the prior from a specific downstream task and fail to generalize to other tasks. Specifically, there is an undesirable trend that these methods perform worse on the classification task than their instance discrimination counterparts, since they are delicatedly tailored for dense predictions and emphasis on the local feature learning.

We argue that a good self-supervised representation learning algorithm should not leverage task-specific priors but learn local representations spontaneously. In this paper, we present a new self-supervised learning approach, **Le**arning **Whe**re to **L**earn (LEWEL) in a pure end-to-end manner. We first regard the spatial aggregation for embeddings of existing SSL methods, *e.g.*, by the global average pooling (GAP), as summations over all spatial pixels weighted by a set of alignment maps. This formulation suggests that we can explicitly control where to learn in SSL by manipulating the alignment maps. Moreover, in contrast to

---

*Corresponding author. [†]Code: https://t.ly/ZI0A.

a) Image-level Self-Supervised Learning.

Global Semantic Vector

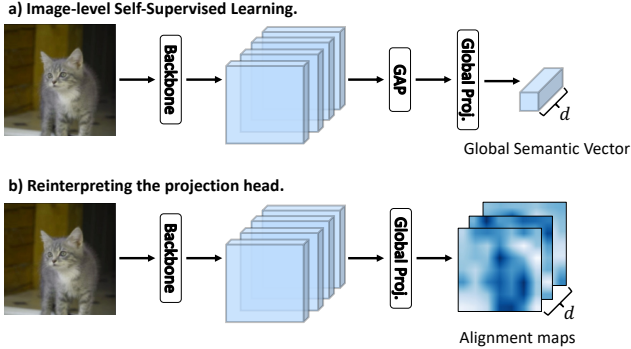**b) Reinterpreting the projection head.**

Alignment maps

Figure 1. **An illustration of the alignment maps prediction**. Based on the standard image-level self-supervised learning, we remove the global average pooling (GAP) layer and reinterpret the global projection as a per-pixel projection, yielding a set of alignment maps that automatically activate to a certain semantic.

previous works manually specifying alignment maps based on downstream rules, our approach learns to just predict the alignment maps on-the-fly during training.

Nevertheless, it is rather challenging to directly model the alignment maps without any supervised signal. Therefore, we propose a novel reinterpretation scheme to guide this process with the help of the global representation. As shown in Fig. 1b, rather than using additional parametrization, we reinterpret the global projection head in SSL as a per-pixel projection to directly predict these alignment maps, which is inspired by the learning paradigm of semantic segmentation [26]. In this way, the global embeddings and the semantic alignment maps are coupled with the weight-sharing projection head. This reinterpretation enables the models to automatically find semantically consistent alignment, yielding a set of spatial alignment maps to "supervise" the alignment process. Actually, the resultant coupled projection head in LEWEL has multiple advantages. On the one hand, based on the generated alignment maps, we can obtain a spectrum of aligned embeddings. Implementing SSL with these embeddings is thus expected to benefit the representation learning since irrelevant nuisances and spatial misalignment have been resolved to a great extent. On the other hand, learning with the aligned embeddings in return facilitates the global representation to extract more truly discriminative features. As a result of this adaptive alignment and coupled projection head, we observe significantly improvements on both image-level and dense predictions simultaneously. Our main contributions are summarized as follows:

1. We introduce a new self-supervised learning approach, **Le**arning **Whe**r**e** to **L**earn (LEWEL), which is a general end-to-end framework and does not involve any downstream task prior for more adaptive and accurate representation learning.

2. In LEWEL, we propose a novel reinterpretation scheme to generate alignment maps with coupled projection

head, thus the aligned and global embeddings can be reciprocal to each other, and, as a result, boost the learned representations.

3. LEWEL brings substantial improvements over prior arts on both image-level prediction and dense prediction. We perform extensive evaluation on linear/semi-supervised classification, semantic segmentation, and object detection tasks, using ImageNet-1K [36], Pascal VOC [11], and MS-COCO [25] benchmarks. Experimental results suggest that LEWEL is able to improve the strong baselines MoCov2 [15] and BYOL [14] under all settings. Specifically, LEWEL improves MoCov2 [15] by 1.6%/1.3%/0.5%/0.4% points, improves BYOL [14] by 1.3%/1.3%/0.7%/0.6% points, on ImageNet linear/semi-supervised classification, Pascal VOC semantic segmentation, and object detection, respectively.

2. Related Works

Learning good representations has long been one of the fundamental questions in computer vision. In recent years, self-supervised learning (SSL) emerged as a promising learning paradigm for representation learning. In general, SSL approaches solve a proxy task to drive the training, including recovering input using auto-encoder [32, 39], generating pixels in the input space [13, 22], predicting rotation [12], and solving a jigsaw puzzle [29]. More recently, contrastive learning methods significantly advanced self-supervised representation learning. The core idea of these approaches is to learn representations invariant to a set of data transformations, *e.g.*, random cropping, random color jittering, and random Gaussian blurring. A large number of contrastive learning approaches [7, 15, 30, 37, 42, 47, 48] are based the the instance discrimination framework, where the models learn to maximize the similarity between positive samples while minimize the similarity between the negative samples. Because instance discrimination relies on a large negative sample size to obtain good performance, some other works proposed to get rid of negative samples by, *e.g.*, incorporating clustering algorithms [1, 3, 4, 23], simply predicting the representation of one augmented view from the other augmented view of the same image [9, 14, 20], feature decorrelation [46], or self-distillation [5]. However, most of the state-of-the-art contrastive learning approaches operate on the global feature only, which risks involving object-irrelevant nuisances and spatial misalignment between different augmented view. The proposed LEWEL framework falls into the category of contrastive learning, addressing the aforementioned drawbacks adaptively.

There have been several researches that dedicated to alleviating these problems. Most of them proposed to maintain the spatial resolution of backbone features and involve the priors of downstream tasks in the pre-training stage. For example, some works performed pixel-level contrastive learn-

ing by matching the most similar pixel [40] or the pixels lie in the neighboring region on the original image [33, 44]; the works of [35, 43] learned to match the representation of the regions that correspond to the same patch in the original image, with the help of RoI Pooling [17]; the work of [19] used a set of pre-computed masks to pool corresponding features for matching. In contrast to these methods using pre-defined matching rules, we propose learning where to learn in self-supervised learning with a set of alignment maps predicted on-the-fly during training. Although the way LEWEL predicts the alignment maps is inspired by the seminal learning paradigm of semantic segmentation [26] (*i.e.*, per-pixel classification), we do not involve any prior of semantic segmentation during pre-training, *e.g.*, by enforcing pixel-level consistency. Furthermore, owing to the reinterpretation of the global projection for predicting alignment maps, LEWEL couples the learning of the global representation and the aligned representation and improves their performance simultaneously, while the others suffer from degraded classification performance.

3. Learning Where to Learn

In this section, we first introduce the generalized spatial aggregation formulation of contrastive learning. Then, we present our methodology, **Le**arning **Wh**er**e** to **L**earn (LEWEL), and finally, we discuss the connections between our method and prior works.

3.1. Generalized spatial aggregation

Notations. Let θ denote model parameters to be optimized and ξ be the momentum parameters that are updated by exponential moving average (EMA) $\xi \leftarrow \alpha\xi + (1 - \alpha)\theta$. Following this notation, we denote the encoder (e.g., ResNet-50 [18]) by f_θ and its momentum counterpart by f_ξ. Besides, we denote the unlabeled training image by x and a set of data augmentation operations (e.g., random crop, color jitter, etc.) as $\mathcal{T}$, which are used to produce augmented views for self-supervised learning.

Global contrastive learning. In most of existing contrastive learning frameworks, each training image is independently transformed by two randomly chosen augmentation operations $t', t'' \in \mathcal{T}$ to obtain $x' = t'(x), x'' = t''(x)$. As shown in Fig. 1a, from the first augmented view x', the encoder f_θ outputs a backbone feature $\mathbf{F}' = f_\theta(x')$. Then the Global Average Pooling (GAP) operates on the feature $\mathbf{F}'$ to obtain the representation $y' = \sum_{i=1}^{H}\sum_{j=1}^{W}\frac{1}{H \times W}\mathbf{F}'_{*,i,j} \in \mathbb{R}^D$, where D, H, W are the number of channels, height, and width of $\mathbf{F}'$, respectively. The representation y' is further transformed by a projection head g_θ to obtain the embedding $z' = g_\theta(y') \in \mathbb{R}^d$ where d is the dimensionality of z'. Likewise, the backbone feature $\mathbf{F}''$, the representation y'' and the embedding z'' can be produced from the second augmented view x''.

by momentum encoder f_ξ, the GAP operation and the the momentum projection head g_ξ. Finally, a self-supervised loss $\mathcal{L}_g = \ell(z', z'')$ is applied on the two embeddings to drive the training, where the instantiation of $\ell(\cdot, \cdot)$ will be presented subsequently.

Learning where to learn. The GAP operation is an effective manner of spatial aggregation and introduces the translation invariance. On the one hand, this invariance is favorable for image-level prediction; on the other hand, averaging over all spatial positions induces object-irrelevant nuisances (*e.g.*, background information) and suffers from the loss of spatial information, which is crucial for spatial-sensitive tasks.

In this paper, we propose learning where to learn in self-supervised learning automatically. The formulation of our method is defined as learning an alignment map $\mathbf{W}' \in \mathbb{R}^{H \times W}$ for spatial aggregation:

$$y' = \mathbf{W}' \otimes \mathbf{F}' = \sum_{i=1}^{H}\sum_{j=1}^{W}\mathbf{W}'_{i,j}\mathbf{F}'_{*,i,j}, \qquad (1)$$

where $\sum_{i=1}^{H}\sum_{j=1}^{W}\mathbf{W}'_{i,j} = 1, \mathbf{W}'_{i,j} \geq 0$, and $y' \in \mathbb{R}^D$. Eq. (1) is a general formulation and allows the model to align the mismatched augmented views, excluding the undesirable nuisances. Furthermore, we can see that the GAP is a special case of Eq. (1) where $\mathbf{W}'_{i,j} = \frac{1}{H \times W}, \forall i, j$, suggesting that our method is able to aggregate both local and global representations in a unified framework by manipulating the alignment map $\mathbf{W}'$.

3.2. Reinterpreting and coupling projection head

Reinterpreting and coupling. For the global contrastive methods, given an input image x', the models output a global representation y' and an embedding $z' \in \mathbb{R}^d$. This embedding z consists of d scalars, of which the kth element records the activation of image x' to the kth semantic. Here, the concept of "semantic" is loosely defined and can represent an object, a pattern, or something else encoded by the model. From this point of view, the projection head g_θ acts like a "classifier" atop the global representation y'. With this notion, our methodology is inspired by the learning paradigm of semantic segmentation, *i.e.*, per-pixel classification [26]. We reinterpret the global projection head g as a per-pixel projection and apply g_θ to the feature before GAP (*i.e.*, $\mathbf{F}'$). Then, as illustrated in Fig. 1b, when fed the first augmented view x', the model outputs $\widetilde{\mathbf{W}}' = g_\theta(\mathbf{F}') \in \mathbb{R}^{d \times H \times W}$, containing a set of heat-maps that record the activation of all $H \times W$ positions to all d semantics. This reinterpretation couples the global projection and the alignment map prediction by **weight sharing** of g_θ, allowing the models to learn a better global representation and aligned representation simultaneously.
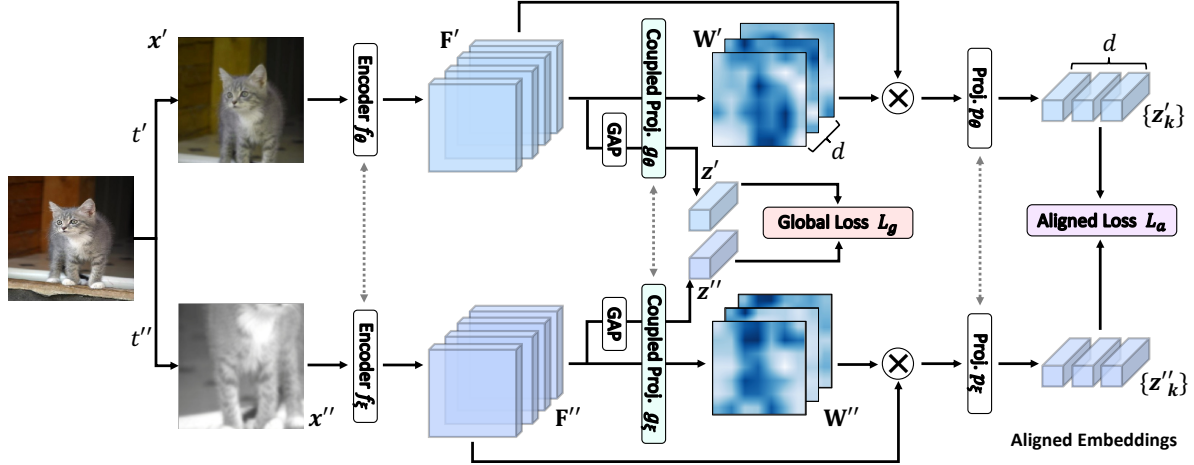
Figure 2. **Overview of the Learning Where to Learn (LEWEL) framework**. Here, θ denotes the model parameters to be learned and ξ is the exponential-moving average of θ. In LEWEL, each random crop of the original images is independently processed by the encoder f, a global average pooling (GAP) layer and a global projector g to produce the global embedding z, upon which the global loss $\mathcal{L}_g$ is applied. In addition, we reinterpret the projection head g as a per-pixel projection to directly predict a set of spatial alignment maps $\mathbf{W}$, *i.e.* coupling the projection head and the alignment map prediction process. Based on the alignment maps, LEWEL adaptively aggregates a spectrum of aligned embeddings $\{z_k\}$ and minimize the aligned loss $\mathcal{L}_a$ on them. The channel grouping scheme is omitted here for clarity.

As in global contrastive learning, the heat-maps $\widetilde{\mathbf{W}}'$ are then ℓ_2-normalized along the *channel* dimension as $\overline{\mathbf{W}}'_{*,i,j} = \frac{\widetilde{\mathbf{W}}'_{*,i,j}}{||\widetilde{\mathbf{W}}'_{*,i,j}||_2}, \forall i, j$, independently for each position. Finally, to obtain the alignment maps $\mathbf{W}'$, we normalize each heat-map from $\overline{\mathbf{W}}'$ independently along *spatial* dimensions as $\mathbf{W}'_k = \mathrm{softmax}(\overline{\mathbf{W}}'_k) \in \mathbb{R}^{H \times W}$, where the softmax function operates on both height and width dimensions, *i.e.*, $\mathbf{W}'_{k,i,j} = \frac{\exp(\overline{\mathbf{W}}'_{k,i,j})}{\sum_{u=1}^{H}\sum_{v=1}^{W}\exp(\overline{\mathbf{W}}'_{k,u,v})}, \forall i, j$.

Channel grouping. Instead of using one alignment map to aggregate one aligned representation, we introduce a grouping scheme that divides the channels of $\mathbf{F}'$ uniformly into h equal-size groups, that is $\mathbf{F}' = [\mathbf{F}'^{(1)}, \cdots, \mathbf{F}'^{(h)}]$ where $[\cdot]$ denotes the concatenation operation. Given the alignment maps $\{\mathbf{W}'_k\}_{k=1}^{d}$, we can accordingly aggregate a set of aligned representations $\{y'_k : y'_k \in \mathbb{R}^D\}_{k=1}^{d/h}$, and

$$y'_k = [\mathbf{W}'_{(k-1)\times h+1} \otimes \mathbf{F}'^{(1)}, \cdots, \mathbf{W}'_{k\times h} \otimes \mathbf{F}'^{(h)}], \forall k, \quad (2)$$

where the operation $\otimes$ is the spatial aggregation operation defined in Eq. (1). We provide the diagram of the grouping scheme in Appendix A.1 for an intuitive illustration. This grouping scheme allows us to explicitly control the number of aligned representations while encoding more semantics into each aligned representation. The aligned representations are then projected by a semantic projector p_θ to obtain the aligned embeddings $\{z'_k : z'_k = p_\theta(y'_k) \in \mathbb{R}^c\}_{k=1}^{d/h}$, where c is the output dimensionality of the projector p_θ. Following the same procedure, the aligned embeddings $\{z''_k\}_{k=1}^{d/h}$ of the second augmented view could be produced according to Eq. (2) and the momentum projectors g_ξ and p_ξ. Finally, a self-supervised loss $\mathcal{L}_a = \frac{h}{d}\sum_{k=1}^{d/h} \ell(z'_k, z''_k)$ is applied on the aligned embeddings to drive the training.

3.3. Implementations

Loss functions. Putting everything together, we formulate the self-supervised learning as minimizing the following objective:

$$\mathcal{L} = (1 - \beta)\mathcal{L}_g + \beta\mathcal{L}_a, \quad (3)$$

where β is the trade-off term between the global loss and aligned loss, which is set to 0.5 by default throughout this paper. The overall pipeline of LEWEL is displayed in Fig. 2 for a more intuitive illustration.

The above formulation is general and is agnostic to the specific choice of the self-supervised loss. Here, we present two instantiations of the loss function. The first variant is termed **LEWEL$_M$** and is based on the InfoNCE loss [30]:

$$\ell_{\mathrm{InfoNCE}}(z', z'') = -\log \frac{e^{\mathrm{sim}(z',z'')/\tau}}{e^{\mathrm{sim}(z',z'')/\tau + \sum_{z^-}\mathrm{sim}(z',z^-)/\tau}}, \quad (4)$$

where $\mathrm{sim}(\cdot, \cdot)$ is the cosine similarity of an input pair, τ is a temperature term, z^- is the embedding of a negative sample. In our implementation, the negative samples are stored in a first-in-first-out queue [15] for the global loss $\mathcal{L}_g$, or consists of embeddings of different images in the current mini-batch for $\mathcal{L}_a$ since the quantity is sufficiently large. Moreover, we present a second variant, termed **LEWEL$_B$**, that does not rely on the negative samples. LEWEL$_B$ adopts the normalized Mean Square Error as in BYOL [14]:

$$\ell_{\mathrm{MSE}}(z', z'') = 2 - 2 \times \mathrm{sim}(q_\theta(z'), \mathrm{sg}(z'')), \quad (5)$$

where sg stands for the stop-gradient operation. The q_θ is an additional predictor that facilitates the learning of the global

representations, while for the aligned representations, a separate predictor s_θ is adopted for the same purpose.

Data augmentations. LEWEL adopts the same configuration of data augmentations as MoCo [15] and BYOL [14]. In general, we first take two random crops from an input image and resize each of them to 224×224. Then the following random distortions are applied on each crop independently with some probabilities: horizontal flipping, color jittering, converting to grayscale, Gaussian blurring, and (for LEVEL$_B$) solarization.

Architecture. We instantiate the encoder $f(\cdot)$ with the ResNet-50 [18], which is the most common choice in this literature. The projectors $g(\cdot)$ and $p(\cdot)$ are implemented by the multi-layer perceptrons (MLPs), with one hidden layer followed by a Batch Normalization [21] (BN) layer and the ReLU [28] non-linear activation. The hidden/output dimension of the projectors $g(\cdot)$ and $p(\cdot)$ are set to 2048/128 for LEWEL$_M$ and 4096/256 for LEWEL$_B$, which means that d is 128/256 for LEWEL$_M$/LEWEL$_B$ and $d = c$ by default. Besides, the extra predictors $q(\cdot)$ and $s(\cdot)$ of LEWEL$_B$ are also instantiated by two-layer MLPs, with the same architecture as the projectors. We follow the settings of MoCo [15] to use the ShuffleBN in the momentum encoder f_ξ. For LEWEL$_B$, we use the EMA BN statistics in the momentum encoder by default for faster training, following [2]. With 400 training epochs, we use the SyncBN for better performance, following BYOL [14].

Optimization. We use the Stochastic Gradient Descent (SGD) with the momentum of 0.9 to minimize our objective functions. For LEWEL$_M$, we use the batch size of 256, initial learning rate of 0.06, weight decay of 10^{-4}, temperature term τ of 0.2, and fix the momentum α of encoder to 0.999. For LEWEL$_B$, we use the batch size of 512, initial learning rate of 1.8, weight decay of 10^{-6}, and set the initial momentum α of the encoder to 0.98, which is increased to 1 according to the cosine schedule [14]. By default, we perform self-supervised pre-training on the ImageNet-1K [36] (IN-1K) datasets using a single machine with eight GPUs. The models are trained for 100/200/400 epochs using the cosine annealing schedule [27] and Automatic Mixed-Precision training on PyTorch [31]. For LEWEL$_B$, the weight decay of bias and BN layers are set to 0. In our ablation studies, we pre-train the models on the ImageNet-100 [37] (IN-100) dataset for fast iteration. In such a case, we simply double the initial learning rate of LEWEL and train the models for 240 epochs following [37] and keep the rest unchanged.

3.4. Discussions

From the spatial alignment perspective. The formulation described in Eq. (1) generalizes to most of prior SSL methods, including the GAP-based approaches and the pixel-based or patch-based approaches. For example, the pixel-based approaches, whose objective is to learn pixel-

Table 1. **Comparison on IN-1K linear classification** with the ResNet-50 models pre-trained on the IN-1K dataset. †: results cited from [9]. ∗: our reproduction.

Method	100 Epochs		200 Epochs		400 Epochs
	Acc@1	Acc@5	Acc@1	Acc@5	Acc@1
InstDisc [42]	-	-	56.5	-	-
PCL [23]	-	-	67.6	-	-
SimCLR [7]	64.6	-	66.6	-	-
SimCLR [7]†	66.5	-	68.3	-	70.4
BYOL [14]†	66.5	-	70.6	-	73.2
SwAV [4]†	66.5	-	69.1	-	70.7
SimSiam [9]†	68.1	-	70.0	-	70.8
MoCov2 [15]∗	64.5	86.1	67.5	88.1	-
BYOL [14]∗	70.6	89.9	71.9	90.4	-
LEWEL$_M$	66.1	87.2	68.4	88.6	-
LEWEL$_B$	**71.9**	**90.5**	**72.8**	**91.0**	73.8

wise correspondence, essentially find a set of one-hot alignment maps that each activates on the single corresponding position only; the patch-based methods take a set of predefined alignment maps that activates the patch regions only for spatial alignment. In sharp contrast to these methods, we propose automatically learning where to learn on the models' own, according to the general formulation Eq. (1). Moreover, since no prior of a specific downstream task is involved in the pre-training stage, LEWEL is able to perform well on both image-level and dense predictions, rather than trading-off the performance of one task to the others'.

From the embedding perspective. For the global contrastive methods, given an input image x, the models output an global embedding $z \in \mathbb{R}^d$. From the embedding perspective, this embedding z consists of d scalars, of which the kth element records the activation of the input images x to the kth semantic. By contrast, guided by the semantic-aware alignment maps, LEWEL (with the number of groups $h = 1$) encodes d aligned embeddings for all semantics accordingly, each of which has a dimensionality of c. In other words, under our framework, more expressive powers are assigned to each semantic by the aligned embeddings, so that the learning on the aligned embeddings implicitly benefits the learning of global embedding z. We will discuss the influence of c in Sec. 4.4.

4. Experiments

4.1. Linear evaluation

Experimental setup. Following prior works [9, 14], we remove the projectors and predictors in LEWEL and train a linear classifier atop the fixed backbone f_θ to evaluate the learned representations. For LEWEL$_M$, we train the linear classifier for 90 epochs with batch size 4,096, initial learning rate 3.2, weight decay 0, LARS optimizer [45] and the cosine annealing schedule [27], following [9]. For

Table 2. **Comparison on IN-1K semi-supervised classification** with the ResNet-50 models pre-trained on the IN-1K dataset. ∗: our reproductions.

Method	Epochs	1% Labels		10% Labels	
		Acc@1	Acc@5	Acc@1	Acc@5
PCL [23]	200	-	75.3	-	86.5
MoCov2 [15]∗	200	43.8	72.3	61.9	84.6
BYOL [14]∗	200	54.8	78.8	68.0	88.5
$LEWEL_M$	200	45.1	71.1	62.5	84.9
$LEWEL_B$	200	**56.1**	**79.9**	**68.7**	**88.9**
SimCLR [7]	1000	48.3	75.5	65.6	87.8
SwAV [4]	800	53.9	78.5	70.2	89.9
BYOL [14]	800	53.2	78.4	68.8	89.0
BarlowTw. [46]	1000	55.0	79.2	69.7	89.3
$LEWEL_B$	400	**59.8**	**83.2**	**70.4**	**90.1**

$LEWEL_B$, we train the classifier for 50 epochs with batch size 256, weight decay 0, SGD optimizer with momentum, learning rate 0.4 that is decayed by a factor of 10 at the 30th and 40th epoch, following [2].

Results. The top1 and top5 validation accuracy on IN-1K are reported in Tab. 1, which includes both cited results and our reproduced results for fair comparisons. Overall, the proposed LEWEL outperforms the state-of-the-art methods under all settings by a substantial margin: with 100 training epochs, $LEWEL_M$/$LEWEL_B$ improve the top1 validation accuracy of their baseline methods MoCo [15]/BYOL [14] by 1.6%/1.3% points; with 400 training epochs, $LEWEL_B$ outperforms BYOL by 0.6% points.

4.2. Semi-supervised classification

Experimental setup. We further evaluate the fine-tuning performance of the self-supervised pre-trained ResNet-50 on subsets of the IN-1K data. For a fair comparison, we use the 1% and 10% subsets that are randomly selected by Chen et al. [7]. We fine-tune the models on these two subsets for 50 epochs with classifier learning rate 1.0 (0.1), backbone learning rate 0.0001 (0.01) for the 1% (10%) subset, which are decayed by a factor of 10 at the 30th and 40th epoch.

Results. The top1 and top5 semi-supervised classification accuracy on the IN-1K validation set are reported in Tab. 2. Using the same pre-training epochs, LEWEL outperforms the other methods by a noticeable margin: in particular, when only 1% of labels are available, $LEWEL_B$ achieves 56.1%/79.9% top1/top5 accuracy, improving the other methods by up to 1.3%/1.1% points under the setting of 200 pre-training epochs. Furthermore, we find that $LEWEL_B$ outperforms state-of-the-art SSL approaches with 2× or more pre-training epochs, e.g., $LEWEL_B$ with 400 epochs perform clearly better than BYOL with 800 epochs. The results of semi-supervised classification and linear classification suggest that LEWEL learns better representations for image-level prediction.

Table 3. **Transfer learning to Pascal-VOC Object Detection and Semantic Segmentation** with models pre-trained on IN-1K datasets. All entries are based on the Faster R-CNN [34] architecture with the ResNet-50 C4 backbone [41]. †: results cited from [9]. ∗: our reproductions.

Method	Epochs	VOC 07+12 Det.			12 Seg.
		AP	AP_{50}	AP_{75}	mIoU
Supervised†	90	53.5	81.3	58.8	67.7
MoCov2 [15]∗	100	56.1	81.5	62.4	66.3
BYOL [14]∗	100	55.5	81.9	61.2	66.9
$LEWEL_M$	100	**56.5**	**82.1**	**63.0**	66.8
$LEWEL_B$	100	56.1	**82.1**	62.3	**67.6**
SimCLR [7]†	200	55.5	81.8	61.4	-
SwAV [3]†	200	55.4	81.5	61.4	-
BYOL [14]†	200	55.3	81.4	61.1	-
SimSiam [9]†	200	56.4	82.0	62.8	-
MoCov2 [15]∗	200	57.0	82.2	63.4	66.7
BYOL [14]∗	200	55.8	81.6	61.6	67.2
$LEWEL_M$	200	**57.3**	82.3	63.6	67.2
$LEWEL_B$	200	56.5	**82.6**	**63.7**	**67.8**

4.3. Transfer learning to other tasks

To evaluate the transfer learning performance of the pre-trained model to other tasks, we use two standard benchmarks: Pascal VOC [11] and MS-COCO [25].

VOC Object Detection and Semantic Segmentation. For object detection, we use the pre-trained model to initialize the ResNet-50-C4 backbone of the Faster-RCNN [34] model. The models are trained on the trainval07 + 12 split (∼16.5k images) and evaluated on the test12 split (∼5k images), using the opensource codebase detectron2 [41]. We follow the standard schedule in [41], i.e., 24k iterations with a batch size of 16, decaying the learning rate at 3/4 and 11/12 of the total steps, and using SyncBN. For the semantic segmentation, we use the dilated FCN [26] model with output stride of 8, which is trained on Pascal VOC 2012 train + aug split (∼10.6k images) and evaluted on the val split (∼1.5k images) using the mmsegmentation [10] codebase. We train the models for 20k iteration with a batch size of 16, SyncBN and the "poly" learning rate schedule [6]. For all models, we search for the best fine-tuning learning rate and report the corresponding results.

The experimental results of object detection (measured by Average Precision (AP), AP_{50}, and AP_{75}) and semantic segmentation (measured by mean-Intersection-of-Union (mIoU)) are summarized in Tab. 3. Though the prior work [8] reported that the linear accuracy is not necessarily related to the performance on downstream task, we observe that LEWEL successfully achieves non-trivial improvements on both object detection and semantic segmentation. In fact, LEWEL outperforms all compared methods on almost all entries, using 100-/200-epoch training budget.

Table 4. **Transfer learning to MS-COCO Object Detection and Instance Segmentation** with models pre-trained for 200 epochs on IN-1K dataset. All entries are based on the Mask R-CNN [16] architecture. †: results from [9]. ∗: our reproduction.

Method	Object Det.			Instance Seg.		
	AP	AP_{50}	AP_{75}	AP	AP_{50}	AP_{75}
`ResNet50-C4:`						
Supervised†	38.2	58.2	41.2	33.3	54.7	35.2
SimCLR [7]†	37.9	57.7	40.9	33.3	54.6	35.3
SwAV [3]†	37.6	57.6	40.3	33.1	54.2	35.1
BYOL [14]†	37.9	57.8	40.9	33.2	54.3	35.0
SimSiam [9]†	37.9	57.5	40.9	33.2	54.2	35.2
MoCov2 [15]∗	38.8	58.0	**42.0**	34.0	55.2	**36.3**
BYOL [14]∗	38.1	58.4	40.9	33.3	55.0	35.3
$LEWEL_M$	**38.9**	58.6	**42.0**	**34.1**	55.3	**36.3**
$LEWEL_B$	38.5	**58.9**	41.2	33.7	**55.5**	35.5
`ResNet50-FPN:`						
DenseCL [40]	40.3	59.9	44.3	36.4	57.0	39.2
ReSim [43]	39.8	60.2	43.5	36.0	57.1	38.6
$LEWEL_M$	40.0	59.8	43.7	36.1	57.0	38.7
$LEWEL_B$	**41.3**	**61.2**	**45.4**	**37.4**	**58.3**	**40.3**
PixelPro [44] (400 ep)	41.4	61.6	45.4	37.4	-	-
$LEWEL_B$ (400 ep)	**41.9**	**62.4**	**46.0**	**37.9**	**59.3**	**40.7**

COCO Object Detection and Instance Segmentation. We adopt the Mask R-CNN [16] architecture with the ResNet50-C4 [41] (following [9, 15]) or ResNet50-FPN [24] (following [40, 43, 44]) backbone, which is pre-trained for 200/400 epochs on ImageNet-1K dataset. All models are fine-tuned on the COCO 2017 `train` split (∼118k images) and finally evaluated on the `val` split (∼5k images). We use a batch size of 16 and adopt the $1\times$ schedule in the detetron2 [41], which uses 90k training iterations in total and decays the learning rate at the 60k-th and 80k-th iteration by a factor of 10. We search the fine-tuning learning rate for LEWEL and the reproduced methods.

The standard COCO metrics, including AP, AP_{50} and AP_{75} for both object detection and instance segmentation, of all methods are reported in Tab. 4. We can see that LEWEL achieves the best performance in terms of all metrics. Concretely, $LEWEL_M$/$LEWEL_B$ consistently improve the strong baselines MoCo/BYOL on all entries by up to 0.5% points. And the gains become even larger when compared with other state-of-the art methods without spatial alignment. Furthermore, compared with the hand-crafted spatial alignment methods [40, 43, 44], our experiments in Appendix B.1 show that LEWEL 1) performs on par with or even better than them on the dense prediction tasks under both $1\times$ and $2\times$ finetuning schedules; 2) significantly outperforms them on classification. These experiments, combined with those on Pascal-VOC benchmark, clearly demonstrate that LEWEL is able to improve the dense prediction performance of self-supervised learning.

Table 5. **The influence of each component** on IN-100 linear classification and transfer learning to VOC 12 semantic segmentation.

Global	Align.	Coupled Head	IN-100 Acc.	VOC Seg. mIoU
✓	×	×	79.5	61.6
×	✓	×	80.0	62.6
✓	✓	×	81.0	62.7
✓	✓	✓	**82.1**	**63.4**

Table 6. **Comparison with MoCo with large projection heads** on IN-100 linear classification and VOC semantic segmentation.

| Method	Extra p_θ	d	IN-100 Acc.	VOC mIoU
MoCov2 [15]	×	128	79.5	61.6
	×	256	79.8	60.6
	×	512	80.2	61.5
	✓	128	79.9	62.2
$LEWEL_M$	×	128	81.8	63.0
$LEWEL_M$ w/ rand. **W**	✓	128	79.8	61.9
$LEWEL_M$	✓	128	**82.1**	**63.4**

4.4. Ablations

Experimental setups. We pre-train all the models on IN-100 dataset, a subset of the IN-1K selected by [37]. The models are evaluated with the linear evaluation and on the semantic segmentation, as described in Secs. 4.1 and 4.3. By default, we use $LEWEL_M$ because it is faster to train.
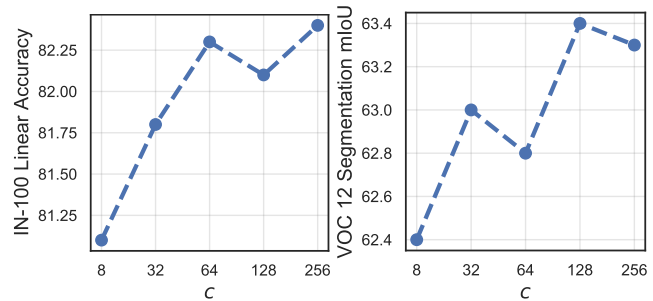
Influence of each component. In Tab. 5, we investigate the contributions of the introduced aligned loss and weight-sharing scheme of the projector g (*i.e.* the coupled head design) to our approach. We can see that, using only the global loss (*i.e.*, the MoCov2 baseline) or aligned loss, the results on the two evaluated tasks are indeed inferior to the variant using both of these two losses. Moreover, the incorporation of the weight-sharing scheme yields the further gains, improving the vanilla baseline by 2.6%/1.8% points in terms of linear classification accuracy/segmentation mIoU. The results verifies the effectiveness of the aligned loss and the coupled head / weight-sharing scheme of LEWEL.

Comparison to MoCov2 with larger/extra projection heads. Since the LEWEL uses a separate projection head for the aligned representation, it is important to clearly identify the contribution of the extra parameters to its performance improvement. In Tab. 6, we compare the $LEWEL_M$ with MoCov2 [15] with larger or extra projection heads. We do not observe significant improvements with neither the larger nor extra projection head for MoCo. Moreover, we notice that a similar study from [46] also suggested that neither deeper nor wider projection head could improve the performance of BYOL. In contrast, switching from MoCo to LEWEL significantly improves the performance on both classification and segmentation, *i.e.*, by 2.6%/1.8% points, respectively. The experiments indicate that the improvement of LEWEL mostly comes from the algorithm itself, not from the slightly increased parameters.
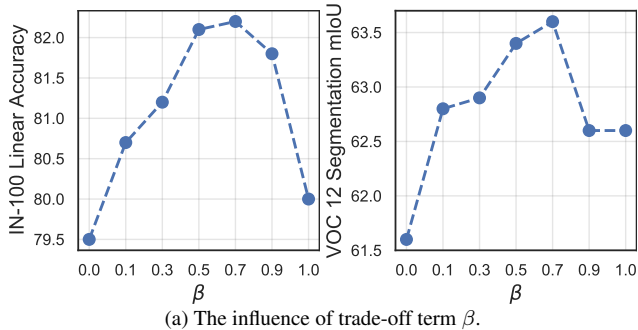
(a) The influence of trade-off term β.   (b) The influence of the dimensionality c of the aligned embeddings.

Figure 3. **Ablation studies** of (a) the loss weight β, and (b) the dimensionality c of the aligned embeddings on IN-100 and VOC 12.

Influence of the loss weight. We also conducted experiments to study to what extent the loss weight β affects the performance of LEWEL, though we fix $\beta = 0.5$ by default for simplicity. The experimental results are shown in Fig. 3a. We observe that, when β is too small (*e.g.*, ≤ 0.3), the models perform relatively worse than those with a large β. When β is set to a larger value, the models actually produce similar results, except for the case of $\beta = 1$. This observation suggests that our reinterpretation of the global projection head and the weight-sharing scheme couple the learning on the global loss and the aligned loss closely, so that the learning of the aligned representations benefits the learning of the global representation.

Influence of the dimensionality of the aligned embeddings. As discussed in Sec. 3.4, each of the aligned embedding is actually an extra representation for a corresponding semantic encoded by the global embedding. In Fig. 3b, we compare the performance of LEWEL$_M$ with different dimensionality c of the aligned embeddings while keep the output dimensionality of the projection head $g(\cdot)$ fixed. From the result, we can see that the performance initially increases w.r.t. the dimensionality c and then stagnates around the point that $c = 64$. The results suggest that the extra expressive power of aligned embedding indeed helps the learning of global representation. However, when the dimensionality is too large, the extra information might be redundant so that the performance will not further increase.

Influence of the number of aligned embeddings. The grouping scheme allows the models to encode richer semantics into each aligned representation while reduces the number of aligned representations. In Tab. 7, we compare the performance of the model variants with different numbers of the aligned embeddings, which are determined by the output dimensionality d of the coupled head $g(\cdot)$ and the number of groups h. Here, we use the LEWEL$_B$ for this study in order to exclude the influence of the negative sample size in LEWEL$_M$. From the table, we have an intriguing observation when fixing $d = 256$: while the linear accuracy increases as h becomes larger and then slight drops, the performance in semantics segmentation exhibits a completely opposite trend that favors a smaller h. This observation may suggest that the aligned representations tend to focus (a) on

Table 7. **The influence of the number of aligned embeddings** on IN-100 linear classification and VOC 12 semantic segmentation.

Method	d	h	IN-100 Acc.	VOC 12 Seg. mIoU
BYOL	256	N/A	81.4	59.7
	512	4	84.6	62.6
	256	1	81.0	63.2
	256	2	82.6	63.3
LEWEL$_B$	256	4	**83.3**	**63.4**
	256	8	83.1	62.1
	256	16	82.9	61.4
	128	4	83.8	60.9
	64	4	84.8	61.8

local regions when the number of aligned embeddings is too large, and (b) on the global content when the number is small. We also find that when $h = 4$, LEWEL$_B$ performs consistently well regardless the value of d. Thus we simply use $d = 4$ for LEWEL$_B$ and adopt $d = 256$ for direct comparison with the baseline BYOL.

Effectiveness of spatial alignments. We report the performance of LEWEL with a random alignment map $\mathbf{W}$ in the second last row of Tab. 6, which is significantly lower than the default one, highlighting the importance of adaptive alignment in LEWEL. Moreover, we visualize the alignment map in Appendix C.1 to show that LEWEL can automatically find semantically consistent alignments.

5. Conclusion

In this work, we present a new approach, Learning Where to Learn (LEWEL), for self-supervised learning (SSL), which is in sharp contrast to existing SSL methods that learn on a fixed (global or local) region. We reinterpret the global projection head in SSL as per-pixel projection, predicting a set of alignment maps to adaptively aggregate spatial information for SSL. As a result of our adaptive alignment and reinterpretation scheme, we observe significantly improvements of LEWEL over the state-of-the-art SSL methods on various tasks, including linear/semi-supervised classification, object detection, and instance/semantic segmentation.

References

[1] Yuki M. Asano, Christian Rupprecht, and Andrea Vedaldi. Self-labelling via simultaneous clustering and representation learning. In *International Conference on Learning Representations*, 2020.

[2] Zhaowei Cai, Avinash Ravichandran, Subhransu Maji, Charless Fowlkes, Zhuowen Tu, and Stefano Soatto. Exponential moving average normalization for self-supervised and semi-supervised learning. In *Proceedings of the IEEE/CVF Conference on Computer Vision and Pattern Recognition*, pages 194–203, 2021.

[3] Mathilde Caron, Piotr Bojanowski, Armand Joulin, and Matthijs Douze. Deep clustering for unsupervised learning of visual features. In *European Conference on Computer Vision*, pages 132–149, 2018.

[4] Mathilde Caron, Ishan Misra, Julien Mairal, Priya Goyal, Piotr Bojanowski, and Armand Joulin. Unsupervised learning of visual features by contrasting cluster assignments. *Advances in Neural Information Processing Systems*, 33, 2020.

[5] Mathilde Caron, Hugo Touvron, Ishan Misra, Hervé Jégou, Julien Mairal, Piotr Bojanowski, and Armand Joulin. Emerging properties in self-supervised vision transformers. *arXiv preprint arXiv:2104.14294*, 2021.

[6] Liang-Chieh Chen, George Papandreou, Iasonas Kokkinos, Kevin Murphy, and Alan L Yuille. Deeplab: Semantic image segmentation with deep convolutional nets, atrous convolution, and fully connected crfs. *IEEE transactions on pattern analysis and machine intelligence*, 40(4):834–848, 2017.

[7] Ting Chen, Simon Kornblith, Mohammad Norouzi, and Geoffrey Hinton. A simple framework for contrastive learning of visual representations. In *International Conference on Machine Learning*, 2020.

[8] Xinlei Chen, Haoqi Fan, Ross Girshick, and Kaiming He. Improved baselines with momentum contrastive learning. *arXiv preprint arXiv:2003.04297*, 2020.

[9] Xinlei Chen and Kaiming He. Exploring simple Siamese representation learning. *arXiv preprint arXiv:2011.10566*, 2020.

[10] MMSegmentation Contributors. MMSegmentation: Openmmlab semantic segmentation toolbox and benchmark. https://github.com/open-mmlab/mmsegmentation, 2020.

[11] M. Everingham, S. M. A. Eslami, L. Van Gool, C. K. I. Williams, J. Winn, and A. Zisserman. The pascal visual object classes challenge: A retrospective. *International Journal of Computer Vision*, 111(1):98–136, Jan. 2015.

[12] Spyros Gidaris, Praveer Singh, and Nikos Komodakis. Unsupervised representation learning by predicting image rotations. In *International Conference on Learning Representation*, 2018.

[13] Ian Goodfellow, Jean Pouget-Abadie, Mehdi Mirza, Bing Xu, David Warde-Farley, Sherjil Ozair, Aaron Courville, and Yoshua Bengio. Generative adversarial nets. In *Advances in Neural Information Processing Systems*, pages 2672–2680, 2014.

[14] Jean-Bastien Grill, Florian Strub, Florent Altché, Corentin Tallec, Pierre Richemond, Elena Buchatskaya, Carl Doersch, Bernardo Avila Pires, Zhaohan Guo, Mohammad Gheshlaghi Azar, et al. Bootstrap your own latent: A new approach to self-supervised learning. *Advances in Neural Information Processing Systems*, 33, 2020.

[15] Kaiming He, Haoqi Fan, Yuxin Wu, Saining Xie, and Ross Girshick. Momentum contrast for unsupervised visual representation learning. In *IEEE Conference on Computer Vision and Pattern Recognition*, pages 9729–9738, 2020.

[16] Kaiming He, Georgia Gkioxari, Piotr Dollár, and Ross Girshick. Mask r-cnn. In *Proceedings of the IEEE international conference on computer vision*, pages 2961–2969, 2017.

[17] Kaiming He, Xiangyu Zhang, Shaoqing Ren, and Jian Sun. Spatial pyramid pooling in deep convolutional networks for visual recognition. *IEEE transactions on pattern analysis and machine intelligence*, 37(9):1904–1916, 2015.

[18] Kaiming He, Xiangyu Zhang, Shaoqing Ren, and Jian Sun. Deep residual learning for image recognition. In *IEEE Conference on Computer Vision and Pattern Recognition*, pages 770–778, 2016.

[19] Olivier J Hénaff, Skanda Koppula, Jean-Baptiste Alayrac, Aaron van den Oord, Oriol Vinyals, and João Carreira. Efficient visual pretraining with contrastive detection. *arXiv preprint arXiv:2103.10957*, 2021.

[20] Lang Huang, Chao Zhang, and Hongyang Zhang. Self-adaptive training: Bridging supervised and self-supervised learning. *arXiv preprint arXiv:2101.08732*, 2021.

[21] Sergey Ioffe and Christian Szegedy. Batch normalization: Accelerating deep network training by reducing internal covariate shift. In *International Conference on Machine Learning*, pages 448–456, 2015.

[22] Diederik P Kingma and Max Welling. Auto-encoding variational Bayes. In *International Conference on Learning Representations*, 2014.

[23] Junnan Li, Pan Zhou, Caiming Xiong, Richard Socher, and Steven CH Hoi. Prototypical contrastive learning of unsupervised representations. In *International Conference on Learning Representations*, 2020.

[24] Tsung-Yi Lin, Piotr Dollár, Ross Girshick, Kaiming He, Bharath Hariharan, and Serge Belongie. Feature pyramid networks for object detection. In *Proceedings of the IEEE conference on computer vision and pattern recognition*, pages 2117–2125, 2017.

[25] Tsung-Yi Lin, Michael Maire, Serge Belongie, James Hays, Pietro Perona, Deva Ramanan, Piotr Dollár, and C Lawrence Zitnick. Microsoft coco: Common objects in context. In *European conference on computer vision*, pages 740–755. Springer, 2014.

[26] Jonathan Long, Evan Shelhamer, and Trevor Darrell. Fully convolutional networks for semantic segmentation. In *IEEE Conference on Computer Vision and Pattern Recognition*, pages 3431–3440, 2015.

[27] Ilya Loshchilov and Frank Hutter. SGDR: Stochastic gradient descent with warm restarts. In *International Conference on Learning Representations*, 2017.

[28] Vinod Nair and Geoffrey E Hinton. Rectified linear units improve restricted Boltzmann machines. In *International Conference on Machine Learning*, 2010.

[29] Mehdi Noroozi and Paolo Favaro. Unsupervised learning of visual representations by solving jigsaw puzzles. In *European Conference on Computer Vision*, pages 69–84. Springer, 2016.

[30] Aaron van den Oord, Yazhe Li, and Oriol Vinyals. Representation learning with contrastive predictive coding. *arXiv preprint arXiv:1807.03748*, 2018.

[31] Adam Paszke, Sam Gross, Francisco Massa, Adam Lerer, James Bradbury, Gregory Chanan, Trevor Killeen, Zeming Lin, Natalia Gimelshein, Luca Antiga, et al. Pytorch: An imperative style, high-performance deep learning library. In *Advances in Neural Information Processing Systems*, pages 8024–8035, 2019.

[32] Deepak Pathak, Philipp Krahenbuhl, Jeff Donahue, Trevor Darrell, and Alexei A Efros. Context encoders: Feature learning by inpainting. In *IEEE Conference on Computer Vision and Pattern Recognition*, pages 2536–2544, 2016.

[33] Pedro O Pinheiro, Amjad Almahairi, Ryan Y Benmalek, Florian Golemo, and Aaron Courville. Unsupervised learning of dense visual representations. *arXiv preprint arXiv:2011.05499*, 2020.

[34] Shaoqing Ren, Kaiming He, Ross Girshick, and Jian Sun. Faster r-cnn: Towards real-time object detection with region proposal networks. *Advances in neural information processing systems*, 28:91–99, 2015.

[35] Byungseok Roh, Wuhyun Shin, Ildoo Kim, and Sungwoong Kim. Spatially consistent representation learning. In *Proceedings of the IEEE/CVF Conference on Computer Vision and Pattern Recognition*, pages 1144–1153, 2021.

[36] Olga Russakovsky, Jia Deng, Hao Su, Jonathan Krause, Sanjeev Satheesh, Sean Ma, Zhiheng Huang, Andrej Karpathy, Aditya Khosla, Michael Bernstein, et al. Imagenet large scale visual recognition challenge. *International Journal of Computer Vision*, 115(3):211–252, 2015.

[37] Yonglong Tian, Dilip Krishnan, and Phillip Isola. Contrastive multiview coding. In *European Conference on Computer Vision*, 2020.

[38] Yonglong Tian, Chen Sun, Ben Poole, Dilip Krishnan, Cordelia Schmid, and Phillip Isola. What makes for good views for contrastive learning? *Advances in Neural Information Processing Systems*, 33:6827–6839, 2020.

[39] Pascal Vincent, Hugo Larochelle, Yoshua Bengio, and Pierre-Antoine Manzagol. Extracting and composing robust features with denoising autoencoders. In *International Conference on Machine Learning*, pages 1096–1103, 2008.

[40] Xinlong Wang, Rufeng Zhang, Chunhua Shen, Tao Kong, and Lei Li. Dense contrastive learning for self-supervised visual pre-training. In *Proceedings of the IEEE/CVF Conference on Computer Vision and Pattern Recognition*, pages 3024–3033, 2021.

[41] Yuxin Wu, Alexander Kirillov, Francisco Massa, Wan-Yen Lo, and Ross Girshick. Detectron2. https://github.com/facebookresearch/detectron2, 2019.

[42] Zhirong Wu, Yuanjun Xiong, Stella X Yu, and Dahua Lin. Unsupervised feature learning via non-parametric instance discrimination. In *IEEE Conference on Computer Vision and Pattern Recognition*, pages 3733–3742, 2018.

[43] Tete Xiao, Colorado J Reed, Xiaolong Wang, Kurt Keutzer, and Trevor Darrell. Region similarity representation learning. *arXiv preprint arXiv:2103.12902*, 2021.

[44] Zhenda Xie, Yutong Lin, Zheng Zhang, Yue Cao, Stephen Lin, and Han Hu. Propagate yourself: Exploring pixel-level consistency for unsupervised visual representation learning. In *Proceedings of the IEEE/CVF Conference on Computer Vision and Pattern Recognition*, pages 16684–16693, 2021.

[45] Yang You, Igor Gitman, and Boris Ginsburg. Large batch training of convolutional networks. *arXiv preprint arXiv:1708.03888*, 2017.

[46] Jure Zbontar, Li Jing, Ishan Misra, Yann LeCun, and Stéphane Deny. Barlow twins: Self-supervised learning via redundancy reduction. *arXiv preprint arXiv:2103.03230*, 2021.

[47] Mingkai Zheng, Fei Wang, Shan You, Chen Qian, Changshui Zhang, Xiaogang Wang, and Chang Xu. Weakly supervised contrastive learning. In *Proceedings of the IEEE/CVF International Conference on Computer Vision (ICCV)*, pages 10042–10051, October 2021.

[48] Mingkai Zheng, Shan You, Fei Wang, Chen Qian, Changshui Zhang, Xiaogang Wang, and Chang Xu. Ressl: Relational self-supervised learning with weak augmentation. *Advances in Neural Information Processing Systems*, 34, 2021.

Table 8. **Comparison with hand-crafted spatial alignment methods**. The experiments on MS-COCO is based on Mask R-CNN architecture with the ResNet-50 FPN backbone and the $1\times/2\times$ schedule [41], following [40, 43, 44].

| Method	Epoch	IN-1K		MS-COCO ($1\times$ Schedule)						MS-COCO ($2\times$ Schedule)					
		Acc@1	Acc@5	AP^b	AP^b_{50}	AP^b_{75}	AP^m	AP^m_{50}	AP^m_{75}	AP^b	AP^b_{50}	AP^b_{75}	AP^m	AP^m_{50}	AP^m_{75}
DenseCL [40]	200	63.6	85.8	40.3	59.9	44.3	36.4	57.0	39.2	41.2	61.9	45.1	37.3	58.9	40.1
ReSim [43]	200	66.1	-	39.8	60.2	43.5	36.0	57.1	38.6	41.4	61.9	45.4	37.5	59.1	40.3
$LEWEL_M$	200	68.1	88.6	40.0	59.8	43.7	36.1	57.0	38.7	-	-	-	-	-	-
$LEWEL_B$	200	**72.8**	**91.0**	**41.3**	**61.2**	**45.4**	**37.4**	**58.3**	**40.3**	**42.2**	**62.3**	**46.1**	**38.2**	**59.6**	**41.1**
PixelPro [44]	400	60.2	83.0	41.4	61.6	45.4	37.4	-	-	-	-	-	-	-	-
$LEWEL_B$	400	**73.8**	**91.7**	**41.9**	**62.4**	**46.0**	**37.9**	**59.3**	**40.7**	**43.4**	**63.5**	**47.7**	**39.1**	**60.7**	**42.4**
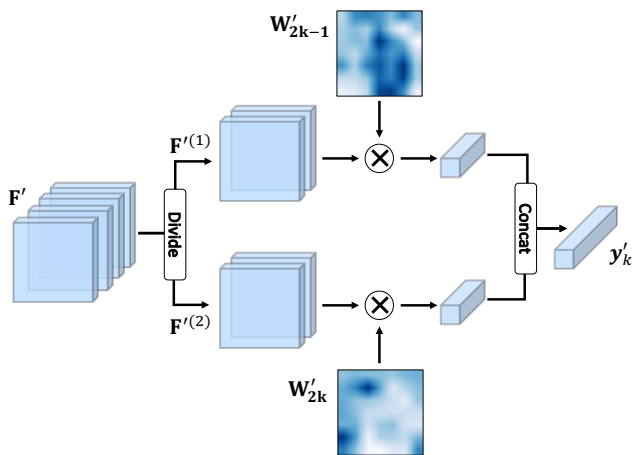
Figure 4. **An illustration of the channel grouping scheme**. Here the number of groups h is set to 2 for simplicity.

A. Additional Illustration of LEWEL

A.1. Illustration of the channel grouping operation.

Instead of using one alignment map to aggregate one aligned representation, we introduce a grouping scheme that divides the channels of $\mathbf{F}'$ uniformly into h equal-size groups, that is $\mathbf{F}' = [\mathbf{F}'^{(1)}, \cdots, \mathbf{F}'^{(h)}]$ where $[\cdot]$ denotes the concatenation operation. Given the alignment maps $\{\mathbf{W}'_k\}_{k=1}^d$, we can accordingly aggregate a set of aligned representations $\{\mathbf{y}'_k : \mathbf{y}'_k \in \mathbb{R}^D\}_{k=1}^{d/h}$, and

$$\mathbf{y}'_k = [\mathbf{W}'_{(k-1)\times h+1} \otimes \mathbf{F}'^{(1)}, \cdots, \mathbf{W}'_{k\times h} \otimes \mathbf{F}'^{(h)}], \forall k, \quad (6)$$

where $\otimes$ is the spatial aggregation operation defined in Eq. (1). For a more intuitive illustration, we summarize the overview of this channel grouping scheme in Fig. 4, where we set the number of groups $h = 2$ for simplicity.

B. Additional Experiment Results

B.1. Comparison with hand-crafted spatial alignment methods

Prior methods [40, 43, 44] are tailored for dense prediction and use pre-defined manual rules to match corresponding pixels. They emphasized on local feature learning and largely ignored the learning of global features that is also important in transferring to both classification and detection tasks (see Sec. 3.4 in [44]). In contrast, LEWEL is a generic method and benefits both image-level and dense predictions. LEWEL leverages the global projection head to predict the spatial alignment maps such that couples the learning of global features and aligned features. Our experimental results in Tab. 8 show that LEWEL significantly outperforms [40, 43, 44] in terms of classification by up to 13% while performing on par with or even better than [40, 43, 44] on detection/segmentation under $1\times/2\times$ training schedule, highlighting the generalization ability of LEWEL.

C. Additional Analyses on LEWEL

C.1. Visualization of the alignment maps.

In Fig. 5, we visualize the alignment maps predicted by $LEWEL_M$ on the ImageNet-1K validation set, which suggest that LEWEL can automatically find semantically consistent alignments for self-supervised learning. Specifically, we observe that the alignment maps may activate on the region of an object (*e.g.*, the visualization in the 3rd column, 1st-2nd rows), the region of multiple objects (*e.g.*, the visualization in the 3rd column, 3rd-4th rows), and on the global region (*e.g.*, the visualization in the 3rd column, 5th-6th rows). The visualization demonstrates that LEWEL is able to learn on both local and global representations simultaneously by manipulating the alignment maps.

C.2. Computational cost.

In Tab. 9, we compare the training time of LEWEL with that of the baselines. The comparison is performed on a single machine with eight V100 GPUs, CUDA 10.1, Py-
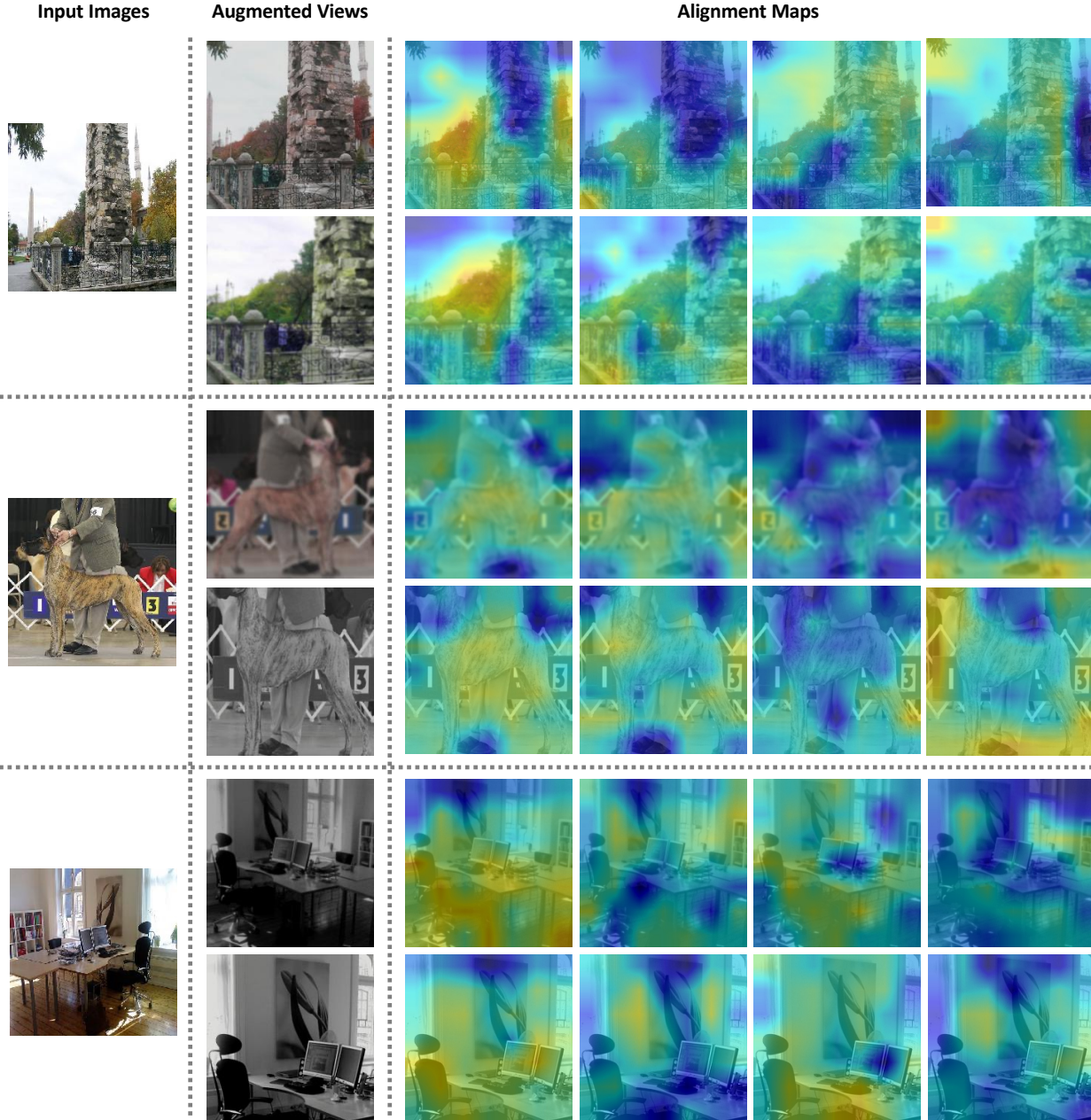
Input Images	Augmented Views	Alignment Maps

Figure 5. **Visualization of the alignment maps** predicted by LEWEL$_M$ on the ImageNet-1K validation set. First column: the input images from the ImageNet validation set. Second column: augmented views generated by random data augmentations. The rest columns: alignment maps predicted by LEWEL$_M$ based on augmented views. The visualization shows that LEWEL automatically finds semantically consistent alignments for self-supervised learning.

Torch 1.8, and the automatic mixed precision (AMP) training[1]. For all methods, we report their training time of one epoch. According to the results in Tab. 9, we can observe that the training time of our method is only marginally increased compared to the baselines. To be more con-

crete, LEWEL$_B$ requires only ∼4% additional overhead compared with BYOL while significantly outperforming BYOL, which demonstrates the efficiency of LEWEL.

C.3. Limitations.

One disadvantage of LEWEL is that the number of aligned representations largely depends on the output di-

---

[1]We find that AMP has little impact on the training time of MoCov2/LEWEL$_M$ but reduces that of BYOL/LEWEL$_B$ by ∼40%.

Table 9. **Training time comparison** on with MoCov2 and BYOL on the ImageNet-1K dataset. The comparison is performed on a single machine with eight V100 GPUs using the automatic mixed precision (AMP) training in PyTorch 1.8.

Method	Training Time/Epoch	Top1 Acc.@200 Epochs
MoCov2	1213s	64.5
LEWEL$_M$	1222s	66.1
BYOL	1141s	70.6
LEWEL$_B$	1191s	71.5

mensionality d of the coupled projection head g. In the cases where d is very large, LEWEL might incur additional training overheads. Nevertheless, we note that our channel grouping scheme can mitigate this drawback by using a larger number of groups to reduce the number of aligned representations.